Egyptian Journal of Chemistry

http://ejchem.journals.ekb.eg/

Highly efficient Co_3O_4/GO adsorbent recycled from spent Lithium-Ion Batteries toward cationic dye from aqueous solutions

Islam K. M. Thabet[1], Abdelaal S. A. Ahmed[1*], Gomaa A. M. Ali[1,2,3*], Zinab H. Bakr[4], Abdelrahman M. Hamed[1],

Adham M Nagiub[1]

[1] *Chemistry Department, Faculty of Science, Al-Azhar University, Assiut 71524, Egypt*
[2] *Faculty of Science, Galala University, Suez, Egypt*
[3] *College of Marine Sciences and Aquatic Biology, University of Khorfakkan, 18119, Sharjah, United Arab Emirates*
[4] *Physics Department, Faculty of Science, Assiut University, Assiut, 71516, Egypt*

Abstract

In this study, the hydrothermal approach was used to extract cobalt oxide (Co_3O_4) nanoparticles and graphene oxide (GO), respectively from the cathode and the anode of spent lithium-ion batteries (LiBs). To gather the benefits of both Co3O4 and GO, the Co_3O_4/GO nanocomposite was prepared via hydrothermal method. The prepared materials have been characterized by Fourier transform infrared (FT-IR), X-ray diffraction (XRD), scanning electron microscopy (SEM), transmission electron microscopy (TEM), and nitrogen adsorption-desorption techniques. The characteristic analysis confirms the successful preparation of Co_3O_4/GO nanocomposite with a BET surface area of 40.42 m2/g. Due to high porous structure, and the presence of GO layers, the prepared Co_3O_4/GO nanocomposite displayed high adsorption capacity toward methylene blue (MB) from the aqueous solution. Various adsorption parameters affecting the overall adsorption efficiency such as pH, adsorbent doses, contact time, and initial MB dye concentrations have been systematically investigated. The highest removal efficiency of MB dye onto the Co_3O_4 and Co_3O_4/GO was achieved at alkaline conditions (pH ≈8.5) with a removal efficiency of 94% and 99%, respectively. The kinetic analysis confirmed that the adsorption of MB dye onto Co_3O_4 and Co_3O_4/GO adsorbents fitted with the pseudo-second order model. The isotherm results indicated that the adsorption of MB dye Co_3O_4 and the Co_3O_4/GO nanocomposite obeyed the Langmuir isotherm model, and the estimated maximum adsorption capacity of the Co_3O_4 and the Co_3O_4/GO nanocomposite are 64.94 and 68.97 mg/g, respectively. This study opens a way for converting waste LiBs components into valuable nanomaterials to be applied for water treatment applications.

Keywords: Recycling; metal oxides; lithium-ion batteries (LiBs); Graphene oxide; hydrothermal method; organic pollutants.

1. Introduction

In modern society, lithium-ion batteries (LiBs) are the most attractive power source for portable electronic products such as cell phones and laptops. LiBs consist of a cathode, anode, separator, and organic electrolyte [1]. A combination of cathode active components ($LiCoO_2$), a binder (polyvinylidene fluoride) (PVDF), an electrical conductor, and other additives make up the cathode electrode, which is made of an aluminium plate. The anode electrode is a copper plate covered with a mixture of carbon graphite, an electrical conductor, some additives, and a PVDF binder [1]. Numerous devices, including mobile phones, digital cameras, some electric cars, and others use LiBs [1]. The LiBs may be able to withstand temperatures of up to 3000 °F. The productivity of LiBs is quite high, as it was 2.05 billion in 2005 rose to 5.86 billion in 2012 globally, and increased to 7.84 billion in 2016 and is still rising [2]. The metal content of spent LiBs includes cobalt, aluminium, lead, and lithium, as well as, the presence of hazardous make them unsafe [3]. Some components of spent LiBs must be recovered or extracted to preserve the environment as well as resources [4,5]. This is because they are difficult to decompose or break down and may cause soil and underground water pollution and release some toxic gases that could affect human health. Cobalt oxide is a main component in cathode of LiBs [1,6]. Usually, metals can be extracted from waste batteries or other sources using a variety of techniques, including hydrometallurgical [7], and pyrometallurgical [8]. In the pyrometallurgical process, used batteries are selectively volatilized at high temperatures, then condensed. It is commonly used in the battery recycling process due to its simplicity; however, some toxic gases are emitted. However, the hydrometallurgical process, which involves

---

*Corresponding author e-mail: abdelaalsaiyd@gmail.com; abdelaalsaiyd@azhar.edu.eg (Abdelaal S.A. Ahmed), gomaasanad@azhar.edu.eg.(Gomaa A.M. Ali).

Received date 08 March 2025; Revised date 22 June 2025; Accepted date 03 July 2025
DOI: 10.21608/ejchem.2025.364725.11379

dissolving battery electrodes in strong acids and then recovering the metal by precipitation, extraction, electrodeposition, or the hydrothermal technique, provides a less harmful way for recovering metal from wasted batteries [9].

Currently, water pollution is considered a serious problem that needs to be taken into consideration to keep our water clean and safe.[10,11] From various pollutants dyes are considered the most common source of water pollution in textile, cosmetics, leather, food, pharmaceutical, paint, varnish, pulp, and paper industries . These dyes harm the aquatic ecosystem by lowering the aesthetic value of water features and obstructing light penetration [12]. Some dyes have toxic, mutagenic properties, and can even cause cancer when combined with their metabolites. These dyes also cause problems for human renal, liver, and nervous system dysfunction. They are difficult to decolorize due to their complicated structure [13,14]. Thus, there is great interest from environmentalists and researchers to remove these harmful compounds from wastewater [15-19]1. Additionally, dyes are thought to be a contributing factor in eutrophication and pollution. There are various methods for treating water-containing dyes including chemical oxidation , adsorption [20,21], and photodegradation [16,17]. Adsorption is the most efficient and cost-effective option for dye recovery from water [22-24]. Because adsorption procedures are affordable, highly successful, and economically viable, they are the most often used of all these approaches [23,25]. The adsorbent materials and their morphologies, which are essential to the total adsorption performance, are the primary problem facing the adsorption process [26,27]. In the last decades, a lot of materials have been used as effective adsorbent materials such as carbons [23,28,29], MOFs [30], metal oxides [31,32], two-dimensional materials,[33] agriculture biowaste materials, [34,35] waste-derived adsorbents,[36]……etc.

Here, Co_3O_4/GO nanocomposite has been prepared from the waste LiBs using a hydrothermal technique to be utilized as adsorbent for MB cationic dye from aqueous solution. The Co_3O_4/GO nanocomposite displayed higher adsorption efficiency (R=99%) than that achieved by pure Co_3O_4 (R=94%). Such higher efficiency is mainly assigned to the presence of GO layers. The isotherm analysis confirms that the adsorption of MB onto the Co_3O_4 and the Co_3O_4/GO nanocomposite obeyed Langmuir isotherm model which indicates a chemical adsorption process. The estimated maximum adsorption capacity of monolayers MB dye onto the Co_3O_4 and the Co_3O_4/GO nanocomposite are 64.94 and 68.97 mg/g, respectively. This study suggests the potential application of Co_3O_4/GO nanocomposite as effective adsorbent for wastewater treatment.

2. Experimental (Materials and Methods)

2.1 Chemicals and reagents

All chemicals used in this study were analytical grade. Sulfuric acid (H_2SO_4), phosphoric acid (H_3PO_4), ammonium hydroxide (NH_4OH), potassium permanganate ($KMnO_4$), sodium nitrate ($NaNO_3$, 99%), sodium hydroxide (NaOH, ≥ 98%, pellets anhydrous), hydrochloric acid (HCl, 37%), hydrogen peroxide (H_2O_2), absolute ethanol (C_2H_6O, ≥ 95%), and methylene blue (MB; $C_{16}H_{18}ClN_3S$, ≥ 95%) were purchased from Merck, Darmstadt, Germany. All preparations in our study have been performed with distilled water obtained from an ultra-pure purifier (Ulupure, resistivity ≥ 18.2 MΩ).

2.2 Extraction Co3O4 from the cathode

Samsung Dead 3.8 V LiBs underwent physical disassembly and separation. After washing the cathode powder in warm water for two hours at 3000 rpm using a magnetic stirrer to get rid of any contaminants, it was dried for twelve hours at 80 °C. After dissolving 2 g of dry powder in 80 mL of 3 M HCl and 5 mL of H_2O_2 as a leaching solution, the mixture was stirred magnetically for two hours at 80 °C. Eq. 1 provides an expression for the leaching process.

$$\mathrm{LiCoO}_{2(s)} + \frac{1}{2}\mathrm{H_2O}_{2\,(l)} + 3\mathrm{HCl}_{(aq)} \rightarrow \mathrm{CoCl}_{2(aq)} + \frac{1}{2}\mathrm{O}_{2\,(g)} + \mathrm{LiCl}_{(aq)} + 2\mathrm{H_2O}_{(aq)} \quad \mathbf{(1)}$$

After that, ammonium hydroxide was slowly added to obtain cobalt hydroxide precipitate as represented by Eq. 2.

$$\mathrm{CoCl_2} + 2\mathrm{NH_4OH} \rightarrow \mathrm{Co(OH)_2} \downarrow + 2\mathrm{NH_4Cl} \quad \mathbf{(2)}$$

After that, the autoclave was placed in an oven set at 150 °C for 4 h, and the suspension solution from **Eq. 2** was added. After being cleaned with distilled water and ethanol, the precipitate was dried for 24 h at 100 °C. To prepare cobalt oxide, the dried sample was calcined for 2 h at 480 °C.

2.3 Preparation of GO from the anode

First, the contaminants have been eliminated, and then the carbon powder from the anode of LiBs was separated and washed with hot distilled water and dried at 100 °C for 12 h. based on the modified Hummer approach [37]. Then, 3 mL of concentrated H_3PO_4 and 27 mL of concentrated H_2SO_4 (V/V ratio 9:1) were combined and agitated for 15 minutes. Next, using a magnetic stirrer, 0.225 g of drying powder was added to the acid mixture mentioned above. After that, 1.32 g of $KMnO_4$ was gradually added to the solution while being guided for 24 h, or until the colour turned dark green. The hue changed to bright green when precisely 0.675 mL of H_2O_2 solution was gradually added to the aforesaid solution in an ice bath while being stirred magnetically. After being cleaned with 10 mL of 30% HCl and distilled water, the resulting powder was dried for 24 h at 100 °C.

2.4 Preparation of Co3O4/GO composite:

Exactly 0.3 g of GO powder was mixed with 70 mL of $CoCl_2$ solution, and the mixture was stirred magnetically for 30 minutes. After that, NH_4OH was gradually added under magnetic stirrer until the $Co(OH)_2$ was fully prepared. Then, the mixture was placed in an autoclave and heated to 160 °C for 4 h. The resulting precipitate was then washed with distilled water, dried at 100 °C for 24 h, and then burnt at 480 °C for 2 h. The obtained material is called Co_3O_4/GO nanocomposite.

2.5 Characterization and measurements

Several techniques were used to characterize the prepared GO and Co_3O_4/GO nanocomposite derived from waste LiBs. FT-IR used to determine the functional groups, and the FT-IR spectrum was obtained in the 4000-400 cm^{-1} regions at a resolution of 2 cm^{-1} on a Nicolet spectrophotometer. The crystal structure was investigated by XRD on a monochromatic Cu-K_α radiation source running at 40 kV. The surface morphology was examined by SEM (JSM 7100F FESEM; Zeiss Ultra Plus). TEM images were obtained by a JEM-2100F field emission microscope (JEOL Ltd., Japan). The surface area was investigated by nitrogen adsorption-desorption on Micromeritics ASAP 2020 HD88 system. The surface area and the pore size distribution were determined by Brunauer-Emmett-Teller (BET) and Barrett-Joyner-Halenda (BJH) models, respectively. The point of zero charge (pHPZC) was determined using the drift method.[38] The experiments were conducted by 20 The point of zero charge (pH_{PZC}) were determined using the drift method.[38] The experiments were conducted by 20 mL of 0.1 M NaNCl solutions with initial pH (pH_i) from 2 to 12 adjusted by 0.1M HCl and 0.1M NaOH solutions. To each solution, 0.05 g of Co_3O_4 and Co_3O_4/GO nanocomposite were added and kept under shaking for 24 h, and then the final pH values (pH_f) of the supernatant liquid were measured. By plotting the pH_i vs. the pH_f, the pH values of the pH_{PZC} were determined. .[44]

2.6 Adsorption MB dye

MB dye adsorption was done in the dark in a 50 mL flask using a magnetic stirrer. The adsorption efficiency of the produced GO and Co_3O_4/GO nanocomposite was examined using the batch adsorption technique, considering the influences of solution pH, contact duration, dye concentration, and adsorbent dosage. At a starting concentration of 50 mg/L, 0.02 g of adsorbent material was combined with 25 mL of dye solution in each experiment. Solutions of 0.1 M HCl and 0.1 M NaOH were used to change the pH of the mixture. A UV-visible spectrophotometer set to 664 nm was used to determine the residual concentration of the MB dye solutions. The removal percent (R) was calculated using **Eq. 3**.

$$R\ (\%) = \frac{C_i - C_f}{C_i} \text{ x } 100 \qquad (3)$$

Where, C_i and C_f are the concentrations of MB in initial and final solutions, respectively. The amount of MB adsorbed q (mg/g) was calculated from the mass balance equation as given by **Eq. 4** .

$$q = \frac{(C_i - C_f)}{W}\ V \qquad (4)$$

Where W (g) is the mass of adsorbent, and V is the dye volume (L).

3. Results and discussion

3.1 Adsorbent characterization

As in Fig. 1, the XRD of the Co_3O_4 after thermal annealing at 480 ˚C for 2 h displayed that all diffraction peaks indexed into the face-cantered cubic Co_3O_4 structures (spacing group Fd3m) (JCPDS No. 96-900-5896) in positions 2θ of 19.04°, 30.34°, 36.93°, 37.64°, 44.92°, 54.79°, 57.51° and, 63.40°. These peaks were associated with the (111), (220), (311), (222), (400), (422), (511), and (440) planes. No traces of other phases or impurities, which undisputedly indicate the formation of single crystalline Co_3O_4. This indicates the successful preparation of cobalt oxide. The broad peak that characterizes GO at 2θ = 9.7° and 41.2° is attributed to (002) and (001) diffraction planes respectively. This indicates successful preparation of GO. From the XRD pattern of Co_3O_4/GO nanocomposite, all diffraction peaks of Co_3O_4 and GO were observed which indicates the successful preparation of Co_3O_4/GO nanocomposite.

The FTIR spectra of the Co_3O_4 and Co_3O_4/GO nanocomposite with and without adsorbed dyes are displayed in **Fig. 1(b,c)**. From the FT-IR spectrum, the band at 3417 cm^{-1} for the O-H groups because of the vibration of water-adsorbed molecules, the peak of Co_3O_4/GO nanocomposite is stronger than the peak of Co_3O_4. Furthermore, both materials are visible at a peak that belongs to the C=C groups and it is situated at 1623 cm^{-1}. The faint band at 582 cm^{-1} in the spectrum may also be caused by the existence of the C-O group in the sample. Strong absorption bands can be seen at 560 and 660 cm^{-1}, due to the vibrations of Co-O stretching in Co_3O_4.[39] The FTIR spectra shows that both materials are loaded with MB dye. Almost all the bands on the material surface are still visible after the adsorption of MB; however, chemisorption is indicated by the O-H band at 3417 cm^{-1}, which is stronger than those before dye adsorption.

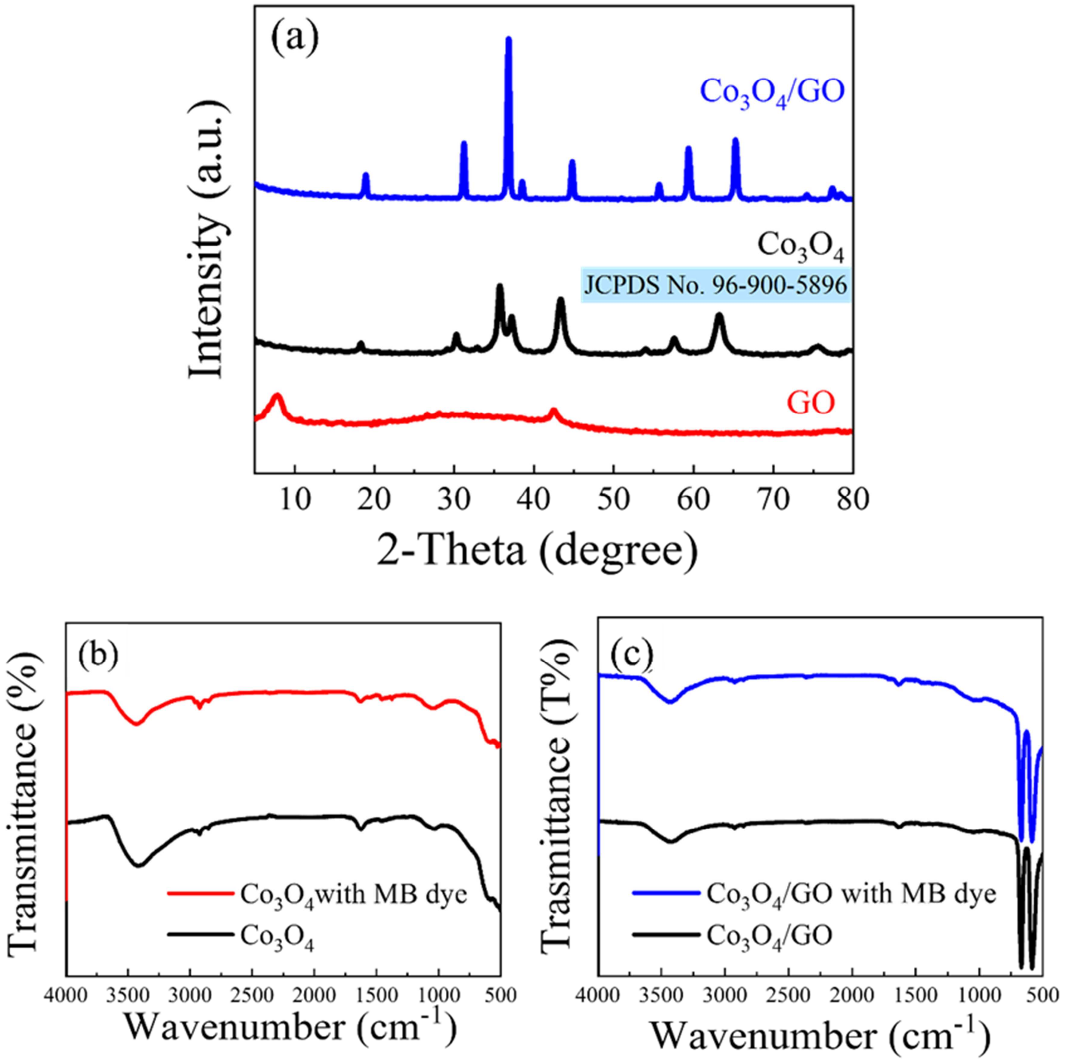

Fig. 1: (a) XRD patterns of Co_3O_4, GO, and Co_3O_4/GO nanocomposite from waste LiBs. FT-IR spectra of (b) Co_3O_4 and (c) Co_3O_4/GO nanocomposite with/without adsorbed MB dye.

TEM images of the Co_3O_4/GO nanocomposite in Fig. 2 (a-c) displayed successful preparation of the Co_3O_4/GO nanocomposite, in which the dark particles represent the Co_3O_4 particles and the transparent layers for the GO layers. The estimated average particle size of Co_3O_4/GO nanocomposite was found to be in the rage from 13.1 to 41.9 nm. On the other hand, SEM analysis was performed to determine the shape and morphology of Co_3O_4/GO nanocomposite under various magnifications and results were depicted in Fig. 2 (d-f). SEM images of the Co_3O_4/GO nanocomposite showed that the Co_3O_4/GO nanocomposite displayed a morphos structure in which the Co_3O_4 particles are loaded into GO layers. This also confirms the successful preparation of Co_3O_4/GO nanocomposite.

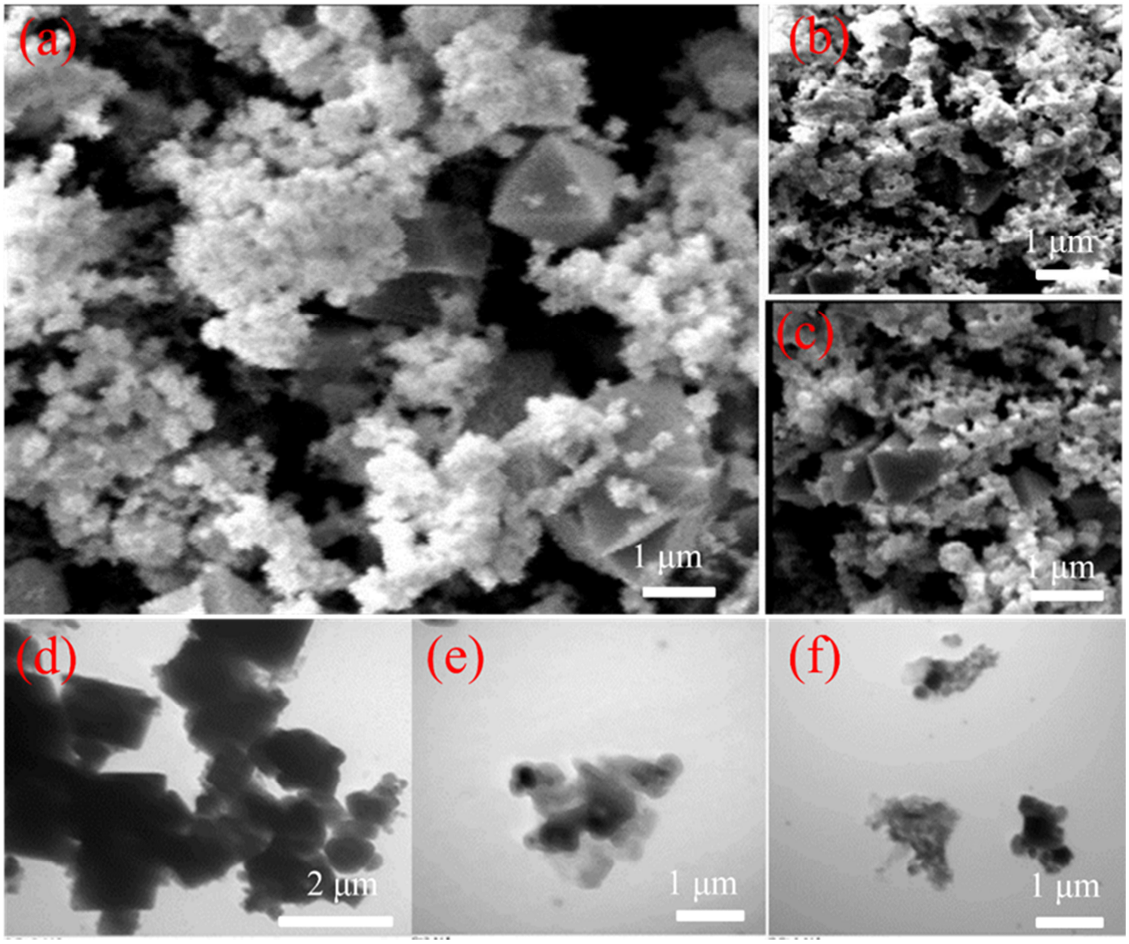

Fig. 2: SEM (a-c) and TEM (d-f) images of Co_3O_4/GO nanocomposite.

As presented in **Fig. 3a**, the nitrogen adsorption-desorption isotherm of the Co_3O_4/GO nanocomposite displayed type-I, which is characteristic of mesoporous materials as stated by the IUPAC categorization.[40] Additionally, the pore size distribution curve in **Fig. 3b** showed that mesopore concentrations are concentrated. The S_{BET} and the pore volume of the Co_3O_4/GO are 40.42 m^2/g, and the mean pore diameter is 8.61 nm.

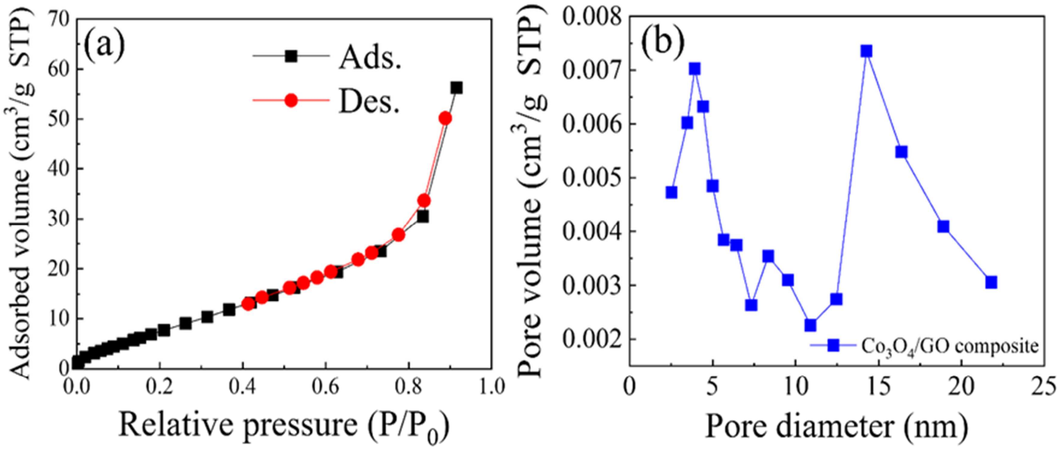

Fig. 3: (a) Nitrogen adsorption-desorption isotherms and (b) pore size distribution of the Co_3O_4/GO nanocomposite.

The pH_{PZC} value is crucial for figuring out the adsorbent's surface charge, which is often influenced by the pH. Thus, throughout the adsorption process, pH_{PZC} is utilized to illustrate the forces of attraction and repulsion between the absorbent and adsorbate. Here, we use the drift approach to calculate the pH_{PZC} based on earlier research.[32] Fig. 4 illustrates how the existence of positive surface charges is shown by the final pH rising as the system's initial pH rises. The pH_{PZC} can be determined by the point of intersection of the final pH line and the initial pH line. The estimated pH_{PZC} values are 7.55 and 7.90 for the Co3O4 and Co_3O_4/GO nanocomposite, respectively. At pH values below pH_{PZC}, the surfaces of the Co_3O_4 and Co_3O_4/GO nanocomposite were positive, while at pH values above pH_{PZC}, the surfaces were negative.

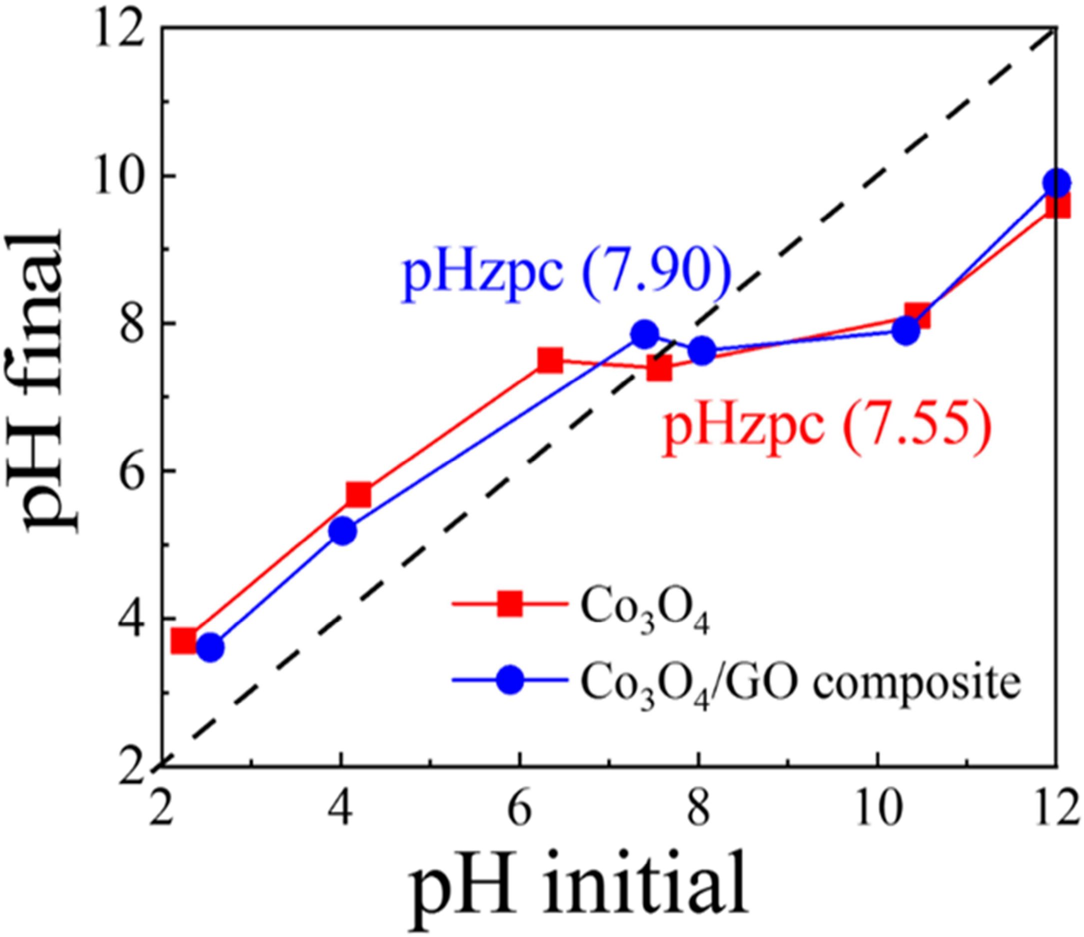

Fig. 4: (a) The pHPZC of the Co_3O_4 and Co_3O_4/GO nanocomposite.

3.2 Adsorption study

3.2.1 Effect of pH

The effect of pH in Fig. 5a shows the removal percentage of MB dye onto Co_3O_4 and Co_3O_4/GO nanocomposite remarkably varies when pH increased from 4 to 11, and the highest removal efficiency was achieved at pH 8.5. This suggests that most of the dyes were eliminated by both materials at basic conditions. For Co_3O_4 and Co_3O_4/GO nanocomposite, the clearance percentages of MB at pH 8.5 were 88% and 97.3%, respectively.

3.2.2 Effect of contact time

The impact of the adsorption duration on the extracted materials' adsorption capability was investigated at a pH of 8.5. The dye solutions were stirred at 300 rpm with 0.02 g of adsorbent material for various time from 15 to 240 minutes. As showed in Fig. 5b, when the contact duration was extended from 15 to 240 minutes, the elimination percentage of MB rose from 17 to 94% for Co_3O_4 and from 44 to 99.8% for Co_3O_4/GO nanocomposite.

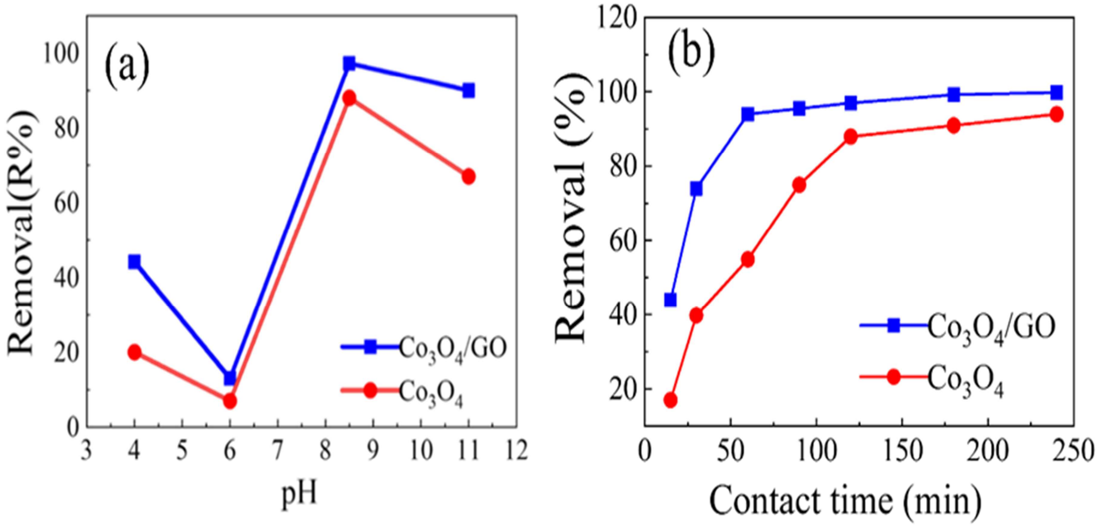

Fig. 5: Effect of (a) solution pH on the removal efficiency of MB dye e from aqueous solution [M= 0.02 g, V= 25 mL, Co = 10 mg/L, t=1h, pH= 4-11] and (b) contact time on the removal efficiency of MB dye. [M= 0.02 g, V= 25 mL, Co = 10 mg L-1, t =15-240 min, pH= 8.5].

3.2.3 Effect of adsorbent dose

After the equilibrium phase is reached, material waste must be avoided by examining the adsorbent dose.[41] **Fig. 6a** displays the results of an experiment that examined the effects of different adsorbent dosages on the dye removal process from aqueous solutions. The adsorption of the MB dye at 10 mg/L is investigated using several adsorbent amounts ranging from 0.002 to 0.02 g at a constant pH of 8.5 and a contact period of 240 minutes. The removal percentage of Co_3O_4 and Co_3O_4/GO nanocomposite for MB dye rose gradually from 38 to 94% and from 86 to 99.80% when the adsorbent dosage was raised from 0.002 to 0.02 g. Accordingly, a larger dose implies greater surface area or active sites which increasing the overall removal efficacy.

3.2.4 Effect of concentration

Fig. 6b illustrates the adsorption capacities of the Co_3O_4 and Co_3O_4/GO nanocomposite at various MB concentrations. By raising the initial dye concentration, adsorption MB capabilities are somewhat increased. The Co_3O_4 and Co_3O_4/GO composite adsorption capabilities rose from 3.13 to 45.64 mg/g and from 3.29 to 49.6 mg/g, respectively, when the concentration increased from 10 to 200 mg/L.

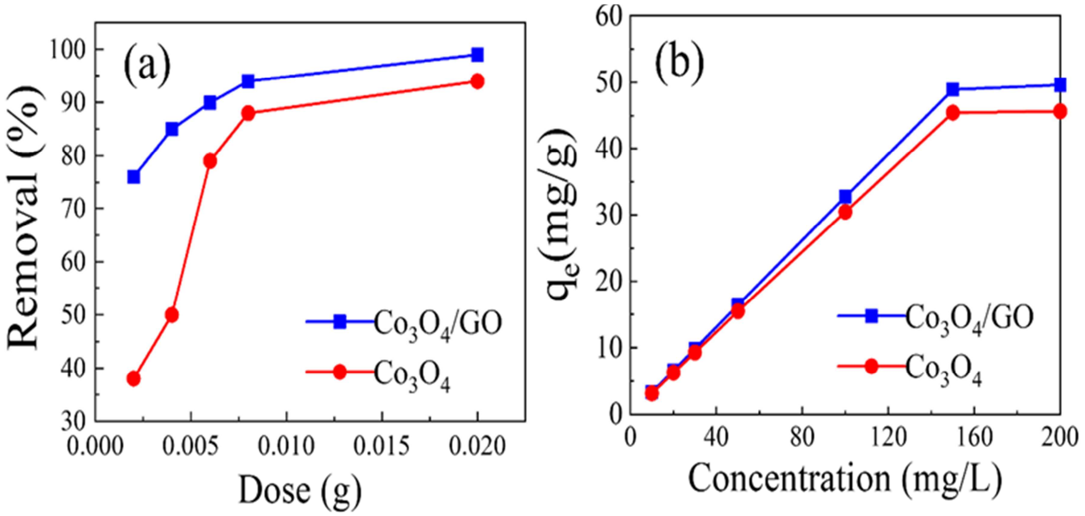

Fig. 6: Effect of (a) dose on MB removal. [M= 0.002-0.02 g, V= 25 mL, Co = 10 mg/L, t = 240 min, pH= 8.5] and (b) initial MB dye concentration. [M= 0.02 g, V= 25 mL, Co = 10-200 mg/L, t= 240 min, pH= 8.5].

3.2.5 Adsorption kinetics

To examine the kinetic behaviour of MB dye adsorption by Co_3O_4 and Co_3O_4/GO nanocomposite, the pseudo-first order and pseudo-second order models were employed to assess the experimental results. The pseudo-second-order (**Eq. 6**) and pseudo-first-order (**Eq. 5**) kinetic models.[42],[43,44]

$$\log(q_e - q_t) = \log q_e - \frac{k_1}{2.303}\ t \qquad (5)$$

$$\frac{t}{q_t} = \frac{1}{q_e^2 k_2} + \frac{t}{q_e} \qquad (6)$$

Where, q_e and q_t are the concentrations of MB in the solution (mg/g) at equilibrium and time t, respectively. k_1 (min^{-1}), the pseudo-first-order adsorption rate constant, k_2 (g/mg. min) the pseudo-second-order adsorption rate constant.

The fitted data are plots in **Fig.7**, and the related kinetic parameters and their correlation coefficients are listed in **Table 1**. It can be observed that the experimental data of MB adsorption onto the Co_3O_4 and Co_3O_4/GO nanocomposite are fitted by the pseudo-second order kinetic model, as indicated by the higher correlation coefficient (R^2) values. The estimated q_e for MB utilizing Co_3O_4 and Co_3O_4/GO nanocomposite were 60 and 70 mg/g, respectively. Furthermore, from the fitted data in **Fig.7** and parameters in **Table 1**, despite the higher R^2 values for the pseudo-second order models, the pseudo-first order models are also displayed higher values (> 0.9), which indicates the presence of both physical and chemical adsorption processes. However, the higher R^2 values demonstrated that the adsorption process mainly followed the pseudo-second-order model.

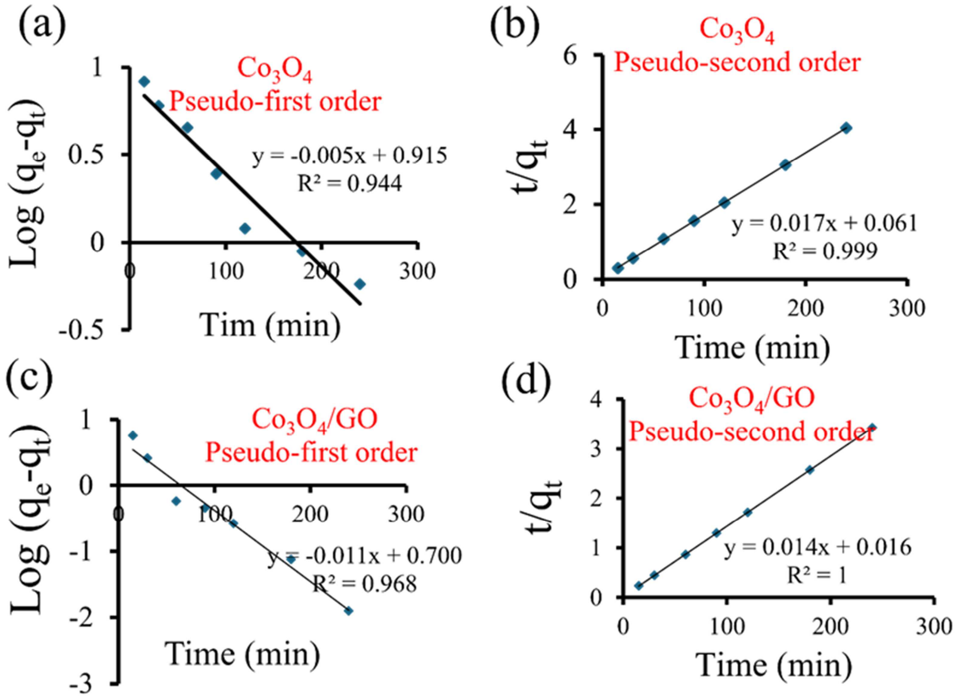

Fig. 7: Pseudo-first order and pseudo-second-order models for the adsorption of MB onto Co3O4 and Co3O4/GO nanocomposite.

Table 1: Parameters of the pseudo-first, pseudo-second-order kinetic models.

Kinetic model	**Parameters**	**Co_3O_4**	**Co_3O_4/GO nanocomposite**
Pseudo-first order	R^2	0.944	0.968
	q_e (mg/g)	8.226	5.014
	k_1 (min^{-1})	-0.012	-0.025
Pseudo-second order	R^2	0.999	1.0
	q_e (mg/g)	60.241	70.422
	k_2 (g/mg.min)	0.004	0.012

3.2.6 Adsorption isotherms

The equilibrium states for dye adsorption on solid surfaces have been described by several mathematical models. The Freundlich and Langmuir models are often used to explain the experimental findings. The Langmuir isotherm model is used for monolayer adsorption on adsorbent surface with a limited number of active sites [43,45,46]. Langmuir model assumes that adsorption occurs on a homogenous surface and that there is no contact between the adsorbates in the surface [47,48]. **Eq. 7** represents the Langmuir isotherm.

$$\frac{1}{q_e} = (\frac{1}{q_{max}k_L})\frac{1}{C_e} + \frac{1}{q_{max}} \qquad (7)$$

Where, k_L is a Langmuir constant associated with the energy of adsorption (L/mg)
and the affinity of the binding sites, and q_{max} (mg/g) is the maximum adsorption capacity.
The Freundlich adsorption isotherm is an equation for a heterogeneous system in which multilayer adsorption may occur on the adsorbent surface [47]. Eq. 8 provides the relationship between equilibrium liquid and solid phase capacity.

$$\log q_e = \log k_f + \frac{1}{n}\log C_e \qquad (\mathbf{8})$$

Where, k_f and n stand for the Freundlich constants. Adsorption process favorability is indicated by the dimensionless constant n; the adsorption capacity is indicated by k_f.

As shown in **Fig. 8** and **Table 2**, the Langmuir and Freundlich isotherms can suit the experimental data of MB adsorption onto Co_3O_4 and Co_3O_4/GO nanocomposite. The Langmuir isotherm model appears to better explain the experimental results based on higher R^2. **Table 2** illustrates that the K_L values for MB adsorption by Co_3O_4/GO nanocomposite are higher than those for adsorption by Co_3O_4. This indicates that Co_3O_4/GO nanocomposite and dye molecule connections are more stable than Co_3O_4 interactions. For MB onto the Co_3O_4 and Co_3O_4/GO nanocomposite, the calculated K_L values are 0.085 and 0.396 L/mg, respectively.

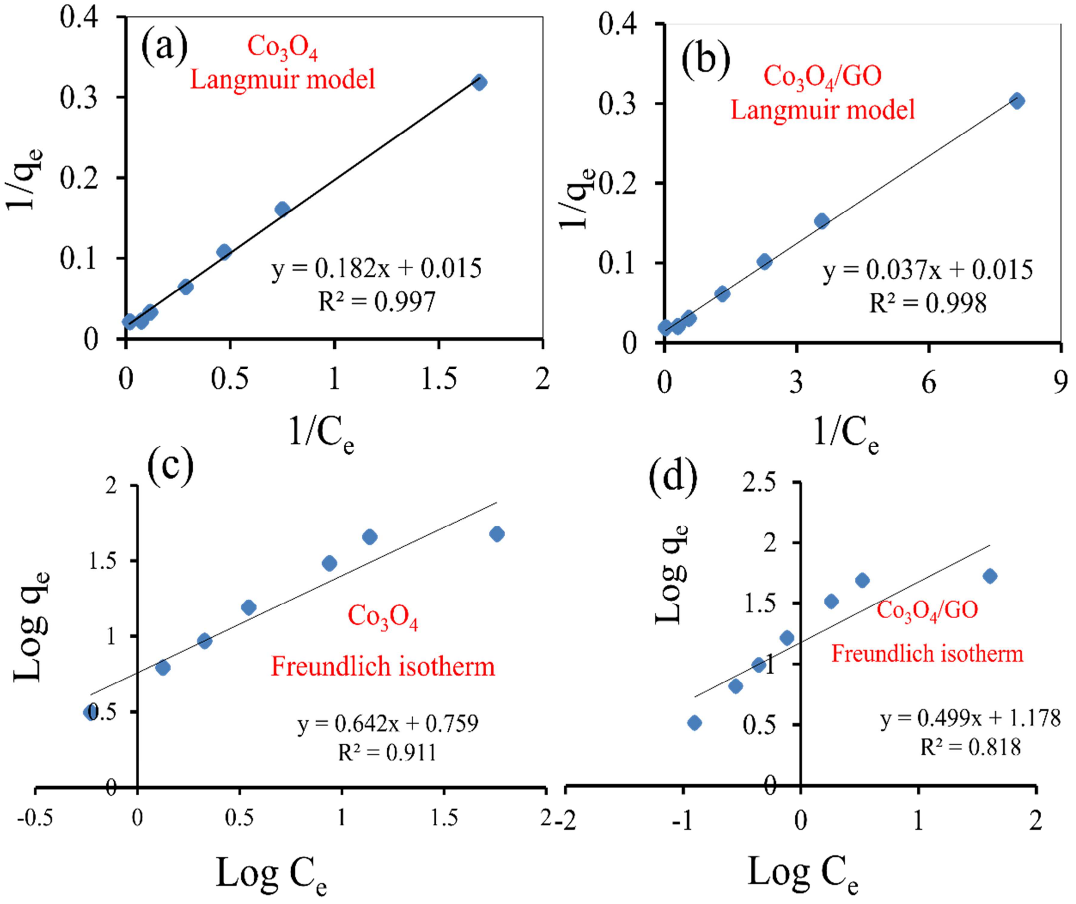

Fig. 8: Langmuir and Freundlich isotherms for adsorption of MB on Co_3O_4 and Co_3O_4/GO nanocomposite.

Table 2: The parameters of Langmuir, and Freundlich isotherms for adsorption of MB onto Co_3O_4 and Co_3O_4/GO nanocomposite

Isotherm model	Parameters	Co_3O_4	Co_3O_4/GO nanocomposite
Langmuir	R^2	0.997	0.998
	q_{max} (mg/g)	64.935	68.966
	K_L (L/mg)	0.085	0.396
Freundlich	R^2	0.911	0.8176
	N	1.558	2.002
	K_f (L/g)	5.742	15.056

Conclusions

In this study, Co_3O_4/GO nanocomposite has been reported from waste LiBs via hydrothermal technique for removal of MB from aqueous solution. The results revealed that the adsorption of MB onto Co_3O_4 and Co_3O_4/GO nanocomposite is strongly controlled by pH, contact time, dye concentration, and adsorbent weight. The maximum adsorption efficiency was achieved at pH of 8.5, and the Co_3O_4 and Co_3O_4/GO nanocomposite showed excellent MB adsorption with a removal efficiency of 94% and 99%, respectively. The adsorption equilibrium of MB onto Co_3O_4 and Co_3O_4/GO nanocomposite was fitted with Langmuir isotherm, as well as the pseudo-second-order kinetic model confirm the chemical adsorption process. The estimated maximum adsorption capacity of the Co_3O_4 and the Co_3O_4/GO nanocomposite are 64.94 mg/g and 68.97 mg/g, respectively. The findings confirmed potential ability to utilize the prepared materials for removal of cationic dyes from aqueous solutions.

Conflict of interest: The authors declare there are no conflicts.

Acknowledgments: The authors thank the Egyptian Academy of Scientific Research and Technology (ASRT, No. 19402).

4. References

1. Ordoñez, J.; Gago, E.J.; Girard, A. Processes and technologies for the recycling and recovery of spent lithium-ion batteries. *Renewable Sustain. Energy Rev.* **2016**, *60*, 195-205, doi:https://doi.org/10.1016/j.rser.2015.12.363.
2. Xu, J.; Thomas, H.R.; Francis, R.W.; Lum, K.R.; Wang, J.; Liang, B. A review of processes and technologies for the recycling of lithium-ion secondary batteries. *J. Power Sources* **2008**, *177*, 512-527, doi:https://doi.org/10.1016/j.jpowsour.2007.11.074.
3. Wang, F.; Sun, R.; Xu, J.; Chen, Z.; Kang, M. Recovery of cobalt from spent lithium ion batteries using sulphuric acid leaching followed by solid–liquid separation and solvent extraction. *RSC Adv.* **2016**, *6*, 85303-85311, doi:10.1039/C6RA16801A.
4. Bakr, H.Z.; Aboelazm, A.A.E.; Khe, C.S.; Ali, A.M.G.; Chong, K.F. Recycling the Spent Lithium-ion Battery into Nanocubes Cobalt Oxide Supercapacitor Electrode. *Curr. Nanosci.* **2024**, *20*, 1-10, doi:http://dx.doi.org/10.2174/0115734137265230231020181833.
5. Aboelazm, E.A.A.; Ali, G.A.M.; Algarni, H.; Yin, H.; Zhong, Y.L.; Chong, K.F. Magnetic electrodeposition of the hierarchical cobalt oxide nanostructure from spent lithium-ion batteries: Its application as a supercapacitor electrode. *J. Phys. Chem. C* **2018**, *122*, 12200-12206, doi:10.1021/acs.jpcc.8b03306.
6. Mei, J.; Liao, T.; Ayoko, G.A.; Bell, J.; Sun, Z. Cobalt oxide-based nanoarchitectures for electrochemical energy applications. *Prog. Mater. Sci.* **2019**, *103*, 596-677, doi:https://doi.org/10.1016/j.pmatsci.2019.03.001.
7. El-Sawaf, A.; A. Tolan, D.; Abdelrahman, M.S.; El-Hay, I.A.; Ismael, M.; Ahmed, A.S.A.; Elshehy, E.A.; Abdu, M.T. Fast synthesis of mesoporous Prussian blue-silica nanocomposite for superior silver ions recovery performance. *J. Chem. Tech. Biotech.* **2024**, *99*, 1941-1954, doi:https://doi.org/10.1002/jctb.7707.
8. Tang, Y.; Zhang, B.; Xie, H.; Qu, X.; Xing, P.; Yin, H. Recovery and regeneration of lithium cobalt oxide from spent lithium-ion batteries through a low-temperature ammonium sulfate roasting approach. *J. Power Sources* **2020**, *474*, 228596, doi:https://doi.org/10.1016/j.jpowsour.2020.228596.
9. Davis, K.; Demopoulos, G.P. Hydrometallurgical recycling technologies for NMC Li-ion battery cathodes: current industrial practice and new R&D trends. *RSC Sustain.* **2023**, *1*, 1932-1951, doi:10.1039/D3SU00142C.
10. Ahmed, A.S.A.; Ali, A.F.M.; Gahlan, A.; El-Sayed, A.-A.Y. Palm leaves -derived porous carbon materials for the elimination of Fe (II) ions from aqueous systems. *Aswan Uni. J. Environ. Stud.* **2025**, *6*, 17-31, doi:10.21608/aujes.2025.333541.1300.
11. Zouli, N.; Maslamani, N.; Hassan, M.; Cheira, M.F.; Hassanein, T.F. Synthesis of novel mesoporous polyvinylamine functionalized with 2-Mercapto-N-methylbenzamide for mercury ions removal from industrial wastewater effluent. *J. Indust. Eng. Chem.* **2025**, *149*, 836-848, https://doi.org/10.1016/j.jiec.2025.02.043.
12. Dutta, P.; Rabbi, M.R.; Abu Sufian, M.; Mahjebin, S. Effects of textile dyeing effluent on the environment and its treatment: A review. *Eng. Appl. Sci. Lett.* **2022**, *5*, 1-1.

13. Angelika, T.; Kamila, M.; Andrzej, P. Synthetic organic dyes as contaminants of the aquatic environment and their implications for ecosystems: A review. *Sci. Total Environ.* **2020**, *717*, 137222, https://doi.org/10.1016/j.scitotenv.2020.137222.
14. Sun, H.-Y.; Gao, Y.-J.; Li, J.-L.; Zou, Y.-M.; Feng, M.-L.; Huang, X.-Y. Removal of Toxic Dyes and Paraquat by a Dual-Functional Metal-Organic Framework. *Chem.Select* **2022**, *7*, e202203826, https://doi.org/10.1002/slct.202203826.
15. Dutta, S.; Gupta, B.; Srivastava, S.K.; Gupta, A.K. Recent advances on the removal of dyes from wastewater using various adsorbents: a critical review. *Mater. Adv.* **2021**, *2*, 4497-4531, doi:10.1039/D1MA00354B.
16. Tolan, D.; El-Sawaf, A.; Ahmed, A.S.A.; Nassar, A.; Mohamed, N.M.; Alhindawy, I.G.; Elshehy, E.A.; Utgikar, V. Enhanced photocatalytic activity of (In–Sr–P) tridoped TiO_2/Bi_2O_3 composite loaded on mesoporous carbon: A facile sol-hydrothermal synthesis approach. *Mater. Chem. Phys.* **2024**, *322*, 129570, https://doi.org/10.1016/j.matchemphys.2024.129570.
17. Li, L.; Zhong, Y.; Hu, Y.; Bai, J.; Qiao, F.; Ahmed, A.S.A.; Ali, G.; Zhao, X.; Xie, Y. Room-temperature synthesis of Ag- and Mn-doped $Cs_2NaBiCl_6$ octahedrons for dye photodegradation. *CrystEngComm* **2023**, *25*, 4355-4363, doi:10.1039/D3CE00372H.
18. Kandil, A.E.-H.T.; Atia, B.M.; El-Dars, F.M.S.E.; Hussein, M.Y.M.; Cheira, M.F. The prospect of using polyvinyl chloride with -n-hydroxyl amine, a metal binding agent, to adsorb uranium from its aqueous solution. *Environ. Nanotech., Monitoring Manag.* **2025**, *23*, 101055, https://doi.org/10.1016/j.enmm.2025.101055.
19. Hendy, M.A.; Kashar, T.I.; Allam, E.M.; Gado, M.A.; Yahia, N.S.; Cheira, M.F. Synthesis of pyridine dicarboxylic acid functionalized and crosslinked to polyvinyl alcohol/polyamide for thorium capturing from aqueous solution. *Chem.Select* **2024**, *9*, e202402329, https://doi.org/10.1002/slct.202402329.
20. El-Sawaf, A.; A. Tolan, D.; Abdelrahman, M.S.; El-Hay, I.A.; Ismael, M.; Ahmed, A.S.A.; Elshehy, E.A.; Abdu, M.T. Fast in-situ synthesis of mesoporous Prussian blue-silica nanocomposite for superior silver ions recovery performance. *J. Chem. Tech. Biotech.* **2024**, *99*, 1941-1954, https://doi.org/10.1002/jctb.7707.
21. Sakr, A.K.; Cheira, M.F.; Hassanin, M.A.; Mira, H.I.; Mohamed, S.A.; Khandaker, M.U.; Osman, H.; Eed, E.M.; Sayyed, M.I.; Hanfi, M.Y. Adsorption of Yttrium Ions on 3-Amino-5-hydroxypyrazole impregnated bleaching clay, a novel sorbent material. *Appl. Sci.* **2021**, *11*, doi:10.3390/app112110320.
22. Han, R.; Wang, Y.; Zou, W.; Wang, Y.; Shi, J. Comparison of linear and nonlinear analysis in estimating the Thomas model parameters for methylene blue adsorption onto natural zeolite in fixed-bed column. *J. Hazard. Mater.* **2007**, *145*, 331-335, https://doi.org/10.1016/j.jhazmat.2006.12.027.
23. Sayed, N.S.M.; Ahmed, A.S.A.; Abdallah, M.H.; Gouda, G.A. ZnO@ activated carbon derived from wood sawdust as adsorbent for removal of methyl red and methyl orange from aqueous solutions. *Sci. Rep.* **2024**, *14*, 5384, doi:10.1038/s41598-024-55158-7.
24. Mohammed, A.M.E.; Kotb, A.; Sanad, M.M.S.; Abdel-Hakim, M.; Ahmed, A.S.A. Enhanced adsorption of carbon sphere by doping with titania nanotubes for crystal violet removal: isotherm, kinetics, and thermodynamic studies. *RSC Adv.* **2024**, *14*, 31332-31347, doi:10.1039/D4RA04889J.
25. Chu, Y.; Zhu, S.; Wang, F.; Lei, W.; Xia, M.; Liao, C. Tyrosine-Immobilized Montmorillonite: An Efficient Adsorbent for Removal of Pb^{2+} and Cu^{2+} from Aqueous Solution. *J. Chem. Eng. Data* **2019**, *64*, 3535-3546, doi:10.1021/acs.jced.9b00304.
26. Thomas, B.; Shilpa, E.P.; Alexander, L.K. Role of functional groups and morphology on the pH-dependent adsorption of a cationic dye using banana peel, orange peel, and neem leaf bio-adsorbents. *Emerg. Mater.* **2021**, *4*, 1479-1487, doi:10.1007/s42247-021-00237-y.
27. Chu, Y.; Khan, M.A.; Xia, M.; Lei, W.; Wang, F.; Zhu, S. Synthesis and mechanism of adsorption capacity of modified montmorillonite with amino acids for 4-Acetaminophenol removal from wastewaters. *J. Chem. Eng. Data* **2019**, *64*, 5900-5909, doi:10.1021/acs.jced.9b00795.
28. Tan, K.B.; Vakili, M.; Horri, B.A.; Poh, P.E.; Abdullah, A.Z.; Salamatinia, B. Adsorption of dyes by nanomaterials: Recent developments and adsorption mechanisms. *Sep. Purif. Tech.* **2015**, *150*, 229-242, https://doi.org/10.1016/j.seppur.2015.07.009.
29. Li, Z.; Sellaoui, L.; Franco, D.; Netto, M.S.; Georgin, J.; Dotto, G.L.; Bajahzar, A.; Belmabrouk, H.; Bonilla-Petriciolet, A.; Li, Q. Adsorption of hazardous dyes on functionalized multiwalled carbon nanotubes in single and binary systems: Experimental study and physicochemical interpretation of the adsorption mechanism. *Chem. Eng. J.* **2020**, *389*, 124467, https://doi.org/10.1016/j.cej.2020.124467.
30. Shayegan, H.; Ali, G.A.M.; Safarifard, V. Amide-Functionalized Metal–Organic Framework for high efficiency and fast removal of Pb(II) from aqueous solution. *J. Inorg. Organometallic Polymers Mater.* **2020**, *30*, 3170–3178, doi:10.1007/s10904-020-01474-0.
31. Li, Y.-Y.; Wu, Y.-L.; Chen, N.; Ma, Y.-L.; Ji, W.-X.; Sun, Y.-G. Preparation of metal oxide-loaded nickel foam adsorbents modified by biochar for the removal of cationic dyes from wastewater. *Chinese J. Analyt. Chem.* **2023**, *51*, 100278, https://doi.org/10.1016/j.cjac.2023.100278.
32. Abdelrazek, E.J.E.; Gahlan, A.A.; Gouda, G.A.; Ahmed, A.S.A. Cost-effective adsorption of cationic dyes using ZnO nanorods supported by orange peel-derived carbon. *Sci. Rep.* **2025**, *15*, 4123, doi:10.1038/s41598-025-86209-2.
33. Younis, S.R.A.; Abdelmotallieb, M.; Ahmed, A.S.A. Facile synthesis of ZIF-8@GO composites for enhanced adsorption of cationic and anionic dyes from their aqueous solutions. *RSC Adv.* **2025**, *15*, 8594-8608, doi:10.1039/D4RA08890E.
34. Ali, A.F.M.; Ahmed, A.S.A.; Gahlan, A.A.; El-sayed, A.-A.Y. Biochar derived from peanut husks as an adsorbent to ammonium ions remediation from aqueous solutions. *Egypt. J. Chem.* **2024**, *67*, 231-244, doi:10.21608/ejchem.2024.271974.9374.

35. T.F. Hassanein, B.K. Binary mixture sorption of basic dyes onto wheat straw. *Bulgarian Chem. Communi.* **2012**, *44*, 131-138.
36. Bakry, A.; Darwish, M.S.A.; Hassanein, T.F. Adsorption of methylene blue from aqueous solutions using carboxyl/nitro-functionalized microparticles derived from polypropylene waste. *Iran. Poly. J.* **2022**, *31*, 185-197, doi:10.1007/s13726-021-00979-w.
37. Hummers Jr, W.S.; Offeman, R.E. Preparation of graphitic oxide. *J. Am. Chem. Soc.* **1958**, *80*, 1339-1339.
38. Putra Hidayat, A.R.; Zulfa, L.L.; Widyanto, A.R.; Abdullah, R.; Kusumawati, Y.; Ediati, R. Selective adsorption of anionic and cationic dyes on mesoporous UiO-66 synthesized using a template-free sonochemistry method: kinetic, isotherm and thermodynamic studies. *RSC Adv.* **2023**, *13*, 12320-12343, doi:10.1039/D2RA06947D.
39. Ali, G.A.M.; Fouad, O.A.; Makhlouf, S.A. Structural, optical and electrical properties of sol–gel prepared mesoporous Co3O4/SiO2 nanocomposites. *J. Alloys Compound.* **2013**, *579*, 606-611, https://doi.org/10.1016/j.jallcom.2013.07.095.
40. Shen, J.; Liu, A.; Tu, Y.; Foo, G.; Yeo, C.; Chan-Park, M.B.; Jiang, R.; Chen, Y. How carboxylic groups improve the performance of single-walled carbon nanotube electrochemical capacitors? *Energy Environ. Sci.* **2011**, *4*, 4220-4229.
41. Hassanin, M.A.; Negm, S.H.; Youssef, M.A.; Sakr, A.K.; Mira, H.I.; Mohammaden, T.F.; Al-Otaibi, J.S.; Hanfi, M.Y.; Sayyed, M.I.; Cheira, M.F. Sustainable remedy waste to generate SiO_2 functionalized on graphene oxide for removal of U(VI) Ions. *Sustain.* **2022**, *14*, doi:10.3390/su14052699.
42. Zhu, H.Y.; Jiang, R.; Xiao, L.; Zeng, G.M. Preparation, characterization, adsorption kinetics and thermodynamics of novel magnetic chitosan enwrapping nanosized gamma-Fe_2O_3 and multi-walled carbon nanotubes with enhanced adsorption properties for methyl orange. *Bioresour Technol* **2010**, *101*, 5063-5069, doi:10.1016/j.biortech.2010.01.107.
43. Mallakpour, S.; Naghdi, M. Design and identification of poly(vinyl chloride)/layered double hydroxide@MnO_2 nanocomposite films and evaluation of the methyl orange uptake: linear and non-linear isotherm and kinetic adsorption models. *N. J. Chem.* **2020**, *44*, 6510-6523, doi:10.1039/D0NJ01162B.
44. Zidan, I.H.; F., C.M.; R., B.A.; and Atia, B.M. Potentiality of uranium recovery from G.Gattar leach liquor using Duolite ES-467 chelating resin: Kinetic, thermodynamic and isotherm features. *Inter. J. Environ. Analyt. Chem.* **2022**, *102*, 2102-2124, doi:10.1080/03067319.2020.1748613.
45. Langmuir, I. The constitution and fundamental properties of solids and liquids. Part I. Solids. *J. Am. Chem. Soc.* **1916**, *38*, 2221-2295.
46. Cheira, M.F. Synthesis of aminophosphonate-functionalised ZnO/polystyrene-butadiene nanocomposite and its characteristics for uranium adsorption from phosphoric acid. *Inter. J. Environ. Analyt.Chem.* **2021**, *101*, 1710-1734, doi:10.1080/03067319.2019.1686493.
47. Freundlich, H. Über die adsorption in lösungen. *Zeitschrift für physikalische Chemie* **1907**, *57*, 385-470.
48. Seaf Elnaser, T.A.; Alotaibi, N.F.; Alruwaili, Y.H.; Gomaa, H.; Sharafeldin, H.; Cheira, M.F.; Abdelmonem, H.A.; Abdelrahman, M.S. Dialdehyde Chitosan/Semicarbazide synthesis for lanthanum, cerium, and neodymium ions recovery from phosphate leachate. *ACS Appl. Poly. Mater.* **2025**, *7*, 6348-6364, doi:10.1021/acsapm.5c00817.